Synthesis Temperature Effect on Na-Mica-4 Crystallinity and Heteroatom Distribution.

Moises Naranjo [1], Miguel A. Castro [2], Agustín Cota [3], Francisco J. Osuna [2], Esperanza Pavón[2] and Maria D. Alba[2,]*

[1] Consejería de Educación. Junta de Andalucía. 41092 Sevilla. Spain

[2] Instituto Ciencia de los Materiales de Sevilla (CSIC-US). Avda. Americo Vespucio, 49. 41092-Sevilla (Spain)

[3] Laboratorio de Rayos X (CITIUS). Avda. Reina Mercedes, 9. 41012-Sevilla (Spain)

ABSTRACT: The discovery of swelling brittle mica, Na-Mica-4, has been one of the most significant advances in the pursuit for a material with high ion-exchange capacity. For technical applications, the control of the phase evolution during the synthesis is crucial. The main aim of this study was to investigate the effect of Na-Mica-4 synthesis temperature on the crystalline phase evolution, Si-Al distribution in the tetrahedral sheet, the Al occupancy between tetrahedral and octahedral sites and their effects on the interlayer space composition. The synthesis temperature range between 600 ºC and 900 ºC was explored. At low temperature (600 ºC), the precursors were transformed in a low-charged swelling 2:1 phyl-

* Corresponding Author: Tel: +34 954489546. Fax: + 34 954460665. E-mail: alba@icmse.csic.es

losilicate, saponite type, which was progressively aluminum enriched with temperature. The high-charged swelling mica was completely formed at 700 ºC, although a minor anhydrous contribution remained up to 850 ºC. Up to 800 ºC, silicates and fluorides secondary phases were detected as a minor contribution.

Keywords: swelling mica, XRD, MAS NMR, charge distribution

Graphical abstract

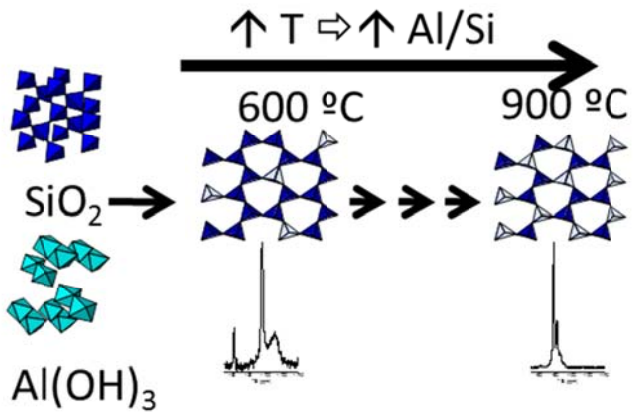

1. Introduction

In recent years, synthetic clays with ion-exchange capacities in the order of 2000 to 4680 $meq \cdot Kg^{-1}$ have been prepared and have been the subject of considerable interest, particularly with respect to their catalytic and adsorption properties [1,2,3,4]. The discovery of swelling brittle mica, Na-Mica-4, has been one of the most significant advances in the pursuit of materials with high ion-exchange capacity (IEC). Unlike true mica, which is a non-expanding silicate with a negative layer charge of one, the Na-Mica-4 readily expands and allows the exchange of interlayer sodium cation [5].

In many cases, solid state synthesis procedures have been used to prepare these materials and fluoride ions have been employed to aid mineralization [6,7,8]. Procedures for synthesizing fine Na-Mica-4 have been refined over a period of time and many starting materials have been tested to achieve the same final product [2,3,9,10,11,12]. Cost effectiveness is one of the main driving forces behind all those attempts.

An important aspect to be considered is the sheet composition and the framework cation ordering, as Si-Al distribution strongly affects the reactivity of layer silicates [13,14]. In this sense, the appropriate characterization techniques are the ^{29}Si and ^{27}Al MAS NMR which are sensible to the local ordering and, therefore, to the Si-Al distribution in the tetrahedral sheet and Al distribution in the framework [15,16]. For some synthetic materials produced at low temperatures, it has been established that the charge density is rather inhomogeneous, hence the intracrystalline reactivity is expected to be non-uniform [17,18]. Moreover, the various compositions and the presence of different phases or impurities may limit the potential uses without pre-treatment [19]. For technical applications, an economi-

cally prized and feasible scalable synthesis method is desirable with an accepted compromise in materials properties. A good way to overcome these problems is to control the phase evolution during the synthesis which could allow optimizing all the synthesis parameters [20,21] (the choice of starting materials [2,3,9,10,11,12], reaction time [22] and temperature settings). For the synthesis of swelling 2:1-layered silicate with a perfectly uniform distribution of isomorphous substitution, the temperature is a key parameter [23] because it needs to be high enough to ensure a true solid solution, melting of one of the component and liquid-liquid miscibility but also preventing the evaporation of fluorine [24,25,26].

The main aim of this study is to investigate the effect of Na-Mica-4 synthesis temperature on the crystalline phase evolution, Si-Al distribution in the tetrahedral sheet, the Al occupancy between tetrahedral and octahedral sites and its effect on the interlayer space composition. The Na-Mica-4 has been synthesized thorough the NaCl-melt method [11] where the nature of starting material, its stoichiometric proportion and the time reaction were fixed and the temperature was a variable factor. As melting point of NaCl is 801 ºC, the range temperature explored was between 600 ºC and 900 ºC with the purposed of testing the influence of temperature and the presence or absence of NaCl-melt fluid. The obtained products were characterized by X-ray diffraction (XRD), thermogravimetric/differential analysis (TG/DTA) and ^{29}Si, ^{27}Al and ^{23}Na solid-state magic-angle-spinning nuclear magnetic resonance (MAS NMR).

2. Experimental

2.1. Materials.

The starting materials were SiO_2 from Sigma (CAS no. 112945-52-5, 99.8 % purity), $Al(OH)_3$ from Rieldel-de Haën (CAS no. 21645-51-2, 99 % purity), MgF_2 from Aldrich (CAS no. 20831-0, 98 % purity), and NaCl from Panreac (CAS no. 131659, 99.5 % purity).

2.2. Synthesis of Na-Mica-4.

A single-step procedure described elsewhere [4], similar to the NaCl-melt method [11] was employed in the synthesis of Na-Mica-4. A stoichiometric powder mixture with the molar composition $4SiO_2$: $2Al_2O_3$: $6MgF_2$: 8NaCl was used.

The reactants mixtures were ground in an agate mortar, weighted, and subsequently heated in a Pt crucible at the temperature range between 600 ºC and 900 ºC for 15 h.

After free cooling, the solids were washed in deionized water and dried at room temperature. The solids were weighted before and after washing. The weight changes relative to the initial mass are expected to shed a light on the synthesis and degradation process of the synthetic mica.

2.3. Sample characterization

Thermal Analysis (TG/DTA) experiments were carried out using a NETZSCH STA 409 PC/PG system, with alumina as the reference. The samples were placed in Pt crucibles and maintained under air throughout the heating period. The temperature was increased at a constant rate of 10 ºC·min^{-1}.

X-ray Diffraction (XRD) patterns were obtained with a Bruker D8 instrument, at the Centro de Investigación, Tecnología e Innovación (CITIUS), Universidad de Sevilla, Sevilla, Spain, using Cu Kα radiation at 40 kV and 40 mA. Diffractograms were obtained from 3º to 70º (2θ) at a scanning speed of $1^{\circ}\cdot min^{-1}$ and a scan step of 0.05º.

Solid State Nuclear Magnetic Resonance (MAS NMR) spectra were recorded on a Bruker DRX400 spectrometer equipped with a multinuclear probe, at the Instituto Ciencia de los Materiales de Sevilla (CSIC-US). Powdered samples were packed in 4 mm zirconia rotors and spun at 10 kHz. ^{29}Si MAS NMR spectra were acquired at a frequency of 79.49 MHz, using a pulse width of 2.7 μs (π/2 pulse length=7.1 μs) and a delay time of 3 s. ^{27}Al MAS NMR spectra were recorded at 104.26 MHz with a pulse widths of 0.92 μs (π/2 pulse length=9.25 μs) and a delay time of 0.5 s. ^{23}Na MAS NMR spectra were recorded at 105.84 MHz with pulse widths of 2.0 μs (π/2 pulse length=12.0 μs) and a delay time of 0.1 s. The chemical shift values are reported in parts per million (ppm) from tetramethylsilane for ^{29}Si, from a 0.1 M $AlCl_3$ solution for ^{27}Al, and from a 0.5 M NaCl solution for ^{23}Na. A modified version of the WinFit program, which handles the finite spinning speed in MAS experiments, was used for the modelling of the spectra [27]. The fit parameters were the chemical shift and full-width at half-height values (fwhh), as well as the area under the curve of the different contributions.

3. Results and discussion

3.1. Gravimetric results.

Fig. 1 shows the weight changes of the products produced in the calcination and washing step as a function of the synthesis temperature. In the calcination step, represented by open square symbols in the Figure 1a, a progressive increasing of the weight loss was observed. The chemical reaction involved in the calcination step, Eq. (1) implied a calculated weight loss of ca. 22 % (dash line, Fig. 1a):

$$8NaCl(s)+ 4SiO_2(s)+ 4Al(OH)_3(s)+ 6MgF_2(s) \rightarrow 4NaCl(s) + Na_4Si_4Al_4Mg_6O_{20}F_4(s) + 4HCl(g) + 8HF(g) \quad (1)$$

At T ≤ 750 ºC, the weight loss was lower than the calculated value from the reaction drawn on eq. I. The formation of the intermediate species and/or the partial conversion of the starting materials could be the responsible. At 750 ºC < T ≤ 800 ºC, the weight loss was similar to the calculated value. However, at T > 800 ºC, the weight loss was higher and, therefore, the simultaneous evaporation of other volatile products (e.g. H_2, Cl_2 ...) could be the responsible of this high weight loss [22].

During the washing step following by filtering, two processes were involved, Eq. (2); the dissolution and removal of NaCl, a calculated weight loss of ca. 21.5 % was expected, and, the hydration of the mica, a calculated weight gain of 5.7 % was expected [2].

$Na_4Si_4Al_4Mg_6O_{20}F_4(s)+4NaCl(s)\rightarrow 4NaCl(aq)+Na_4Si_4Al_4Mg_6O_{20}F_4\cdot 2.7H_2O(s)$ (2)

During washing and filtering, Fig. 1b, a progressive decrease on the weight loss was attained and three regions could be distinguished. At T≤ 750 ºC, the weight loss was higher that the corresponding to the NaCl removal (dotted line on Fig. 1b) which indicates the presence of other soluble phases on the reaction products at these temperatures. At 750 ºC < T ≤ 800 ºC, the weight loss was almost due to the NaCl removal without evidence of the sample hydration. However, at T > 800 ºC, the weight loss was found to be smaller than the expected for NaCl removal, meaning that mica hydration is taking part of the total reaction.

3.2. Framework structure evolution.

3.2.1. X-ray diffraction.

Fig. 2 shows the X-ray diffractograms obtained for the different products and the stick patterns of a set of crystalline phases accounting for the experimental data. The product obtained at the lower temperature (600 ºC) exhibited a XRD pattern that could be described as the result of reflections arising from a hydrated smectite with a broad *001* reflection at 7.35º 2θ that corresponded to a d_{001} = 12.25 Å and a *060* reflection typical of its trioctahedral nature, d_{060}= 1.53 Å (60.5º 2θ) [28]. The typical saw-tooth *hk* bands [29] and *060* reflections of saponite [28] persisted up to 775 ºC. At 650 ºC, the reflections of anhydrous high charged mica (PDF 00-25-842), with a *001* reflection at 9.30º 2θ, started to emerge. In

the range between 700 ºC and 850 ºC it became a minor contribution that accompanied to the main one, the hydrated high-charged mica (Na-Mica-4, PDF 00-54-1025) [4]. The hydrated mica showed a *001* reflection at 7.35º 2θ (d_{001}= 12.25 Å), corresponding to interlayer monovalent cations surrounded by a single water sheet. For T > 850 ºC, the silicate was completely hydrated and the *001* reflection at 9.30º 2θ was no longer observed.

Up to 750 ºC, a large amounts of aluminium oxide fluoride is involved in the product of synthesis. And up to 800 ºC, the XRD patterns exhibited small reflections due to two types of impurities: silicates and fluorides (Fig. 2, Table 1). The nature of theses impurities can explain the evolution of the weight loss observed in the previous section. The presence of solid phases containing fluorides (norbergite, aluminum oxide fluoride and neighborite) and chlorosilicate (sodalite) in the reaction products could be the responsible of the low weight loss observed by gravimetric measures at those temperatures in the calcination step (Fig. 1a) and after the washing step (Fig. 1b).

Moreover, at T > 800 ºC, the presence of hydrated mica and the absence of the others impurities were the responsible of the small weight loss observed by gravimetric measures after the washing step (Fig. 1b).

3.2.2.^{29}Si and ^{27}Al MAS NMR.

Fig. 3 shows the ^{29}Si and ^{27}Al MAS NMR spectra obtained for the synthesized products in the temperature range between 600 ºC and 900 ºC.

The ^{29}Si MAS NMR spectrum for the T=600 ºC showed three set of peaks: a narrow and small peak at ca. - 61.8 ppm, that can be attributed to Q^0 environments, an intense peak at

ca. -95 ppm with a small shoulder at higher frequency, coming from Q^3 Si environments, and a very broad peak at ca. -100 ppm that correspond to Q^4 Si environments [30]. The spectrum's deconvolution helps in the interpretation of this result (see Table 2 and Suppl. 1). Based on the XRD results, an assignation of the spectrum contributions were carried out. The Q^0 site corresponded to the forsterite phase observed by XRD [31]. Moreover, Q^3 Si environment could be deconvoluted in two contributions at -95.3 ppm and -89.0 ppm assigned to Q^3(0Al) and Q^3(1Al) with a chemical shift and relative intensity typical of saponite [32]. Finally, the Q^4 environment corresponded to an amorphous tectosilicate, non-visible by XRD that remained up to 650 ºC. This first assignation at 600 ºC was corroborated by the ^{27}Al MAS NMR spectrum which exhibited aluminum signal in tetrahedral coordination (ca. 67 ppm) due to $Al(OSi)_3$ environment [33] and aluminum signal at ca. 0 ppm, hexacoordinated aluminum, from the aluminum oxide fluoride detected by XRD [34].

As the synthesis temperature increases, the evolution of the two sets of peaks is unalike. On the one hand, the intensity of the Q^0 Si environment of forsterite diminished between 600 ºC and 650 ºC and at 700 ºC it was absent in concordance with XRD pattern where non crystalline nesosilicates phases (forsterite or norbergite) were observed (Fig. 2, Suppl. 1). At $T \geq 750$ ºC, the Q^0 Si environment was again observable and it remained up to 900 ºC although the norbergite phase was no longer visible in the XRD pattern at $T > 800$ ºC.

On the other hand, the Q^3 Si environment region evolved to a large number of peaks between -70 to -95 ppm due to the combination of Q^3 (mAl) ($3 \leq m \leq 0$) environments of mica [4] and Q^4(4Al) from sodalite [35] (See Table 2 for assignment). ^{27}Al MAS NMR spectra supported this assignation, showing a narrow signal at 64.4 ppm [36] due to sodalite phase overlapped with a broad signal at 67.1 ppm due to $Al(OSi)_3$ environment of layered

silicates [33]. Sodalite environment remained up to 800 ºC, which was also evident in the ^{27}Al MAS NMR spectra.

Between 700 ºC and 900 ºC, Q^3(3Al) signal was progressively more intense and it shifted to higher frequency as a consequence of an aluminum enrichment of the mica tetrahedral sheet [15]. It was also corroborated by the increasing of the Al^{IV}/Al^{VI} ratio in the ^{27}Al MAS NMR spectra. The intense Al^{VI} signal in the spectra up to 750 ºC could be explained as due to the aluminum oxide fluoride phase detected by XRD. The remaining broad and small signal at ca. 0 ppm in the temperature range between 800 ºC and 900 ºC belonged to the octahedral aluminum in the mica phase [4]. At T ≥ 775 ºC, a fifth peak at ca. -75 ppm was observed in the ^{29}Si MAS NMR spectra which was interpreted by Alba et al. [4] as due to Lowentein's law violation in high-charged mica but also this resonance could be due to Q^2 Si(2Al) present at the layer edges of the micas [37].

3.3. Interlayer space evolution

3.3.1. Thermal analysis (TG/DTA).

The weight loss measured by TG/DTA between room temperature and 250 ºC is a good estimation for the interlayer water present in layered silicates [38]. Table 3 shows the mass loss and the dehydration temperature as a function of the calcination temperature.

At 600 ºC, two endothermic peaks at 32.6 ºC and 61.9 ºC were observed and they are due to surface water evaporation and low bonding interlayer water; the weight loss was very small in comparison with those observed by hydrated Na-Mica-4 [2].

For higher temperature, only a dehydration temperature was observed between 69.4 ºC and 81.7 ºC which involved a greater weight loss, between 3.0 % and 6.9 %. The dehydration temperature and weight loss increased with the temperature calcination as consequence of: (i) a higher amount of high-charged swelling mica [22], as seen by XRD, and, (ii) a progressively increasing in the total layer charge of mica, as seen by ^{29}Si MAS NMR [5]. The second factor was already reported by Mackenzie [39] who observed that the influence of the layered surface on hydration predominates for lager divalent and monovalent cations in the interlayer space of montmorillonites.

A maximum weight loss of 6.9 % was observed at 900 ºC, as previously observed in fully hydrated Na-Mica-4 [4].

3.3.2. ^{23}Na MAS NMR

The ^{23}Na MAS NMR spectrum of the sample synthetized at 600 ºC, Fig. 4, showed a broad asymmetric band between 20 and -60 ppm and a small peak at 37.2 ppm assigned to non-exchangeable sodium [40]. The broad band was deconvoluted in four peaks (Table 4) centred at 3.7 ppm (3.6 %) due to sodalite [35], and at -10.1 ppm, -21.1 ppm and -33.2 ppm due to fully hydrated, poorly hydrated and dehydrated exchangeable sodium, respectively [40,41]. In this sample, the non-exchangeable sodium accounted a 6.4 % of the total interlayer sodium in the 2:1 phyllosilicate.

The line shape of the spectra with temperature was similar to the above; the line width and intensity of the peaks were the only changes. The peak at ca. 4 ppm, sodalite, increased

progressively up to 775 ºC and after it diminished drastically. In fact, this phase was not detected in the XRD patterns after 800 ºC or in the ^{29}Si MAS-NMR spectra.

Regarding to the interlayer sodium, two facts were remarkable: (i) the peak at ca. 37 ppm, non-exchangeable sodium, increased up to 775 ºC and after it diminished up to be negligible at 900 ºC (0.5 %), and, (ii) the band that includes all type of exchangeable sodium narrowed as temperature increased. The Table 3 summarizes the evolution of the hydration of exchangeable sodium. The amount of fully hydrated sodium increased with temperature, in good agreement with the weight loss evolution observed by TG/DTA. The sample synthesized at 775 ºC was the only exception but the weight loss at this temperature didn´t increase respect to the 700 ºC (Table 3).

Signal from the other Na-containing phase, $NaMgF_3$, observed by XRD, were no detected in the ^{23}Na spectra [22].

4. Conclusions

The results have helped to clarify the synthesis mechanism of high-charged swelling mica, to identify the intermediate compounds and to analyze the effect of temperature in framework cations distribution.

At low temperature (600 ºC), the precursors were transformed in a low-charged swelling 2:1 phyllosilicate, saponite type, which was progressively aluminum enriched with temperature. The high-charged swelling mica was completely formed at 700 ºC, although a minor anhydrous contribution remains up to 850 ºC. Up to 800 ºC, silicates and fluorides secondary phases were present as a minor contribution,

As the high-charged mica was enriched in tetrahedral aluminum, higher layer charge, the hydration of interlayer cation increased and the non-exchangeable interlayer sodium decreased.

Acknowledgments

The authors wish to acknowledge the Junta de Andalucía (Spain) and FEDER (Proyecto de Excelencia de la Junta de Andalucía, project P12-FQM-567) for providing financial support.

References

[1] Y. Morikawa, T. Goto, Y. Morooka, T. Ikawa, Chem. Lett. (1982) 1667-1670.

[2] M. Gregorkiewitz, J. A. Rausell-Colom, Am. Mineral. 72 (1987) 515-527.

[3] W. J.Paulus, S. Komarneni, R. Roy, Nature 357 (1992) 571-573.

[4] M. D.Alba, M. A, Castro, M. Naranjo, E. Pavón, Chem. Mater. 18 (2006) 2867-2872.

[5] E. Pavón, M. A. Castro, M. Naranjo, M. M. Orta, M. C. Pazos, M. D. Alba, Am. Miner. 98 (2013) 394-400.

[6] H. Tateyama, S. Nishimura, K. Tsunematsu, K. Jinnai, Y. Adachi, M. Kimura, Clays Clay Miner. 40 (1992) 180-185.

[7] K. Kitajima, F. Koyama, N. Takusagawa, Bull. Chem. Soc. Jpn. 58 (1985) 1325-1326.

[8] F. D. Duldulao, J. M. Burlitch, Chem. Mater. 3 (1991) 772-775.

[9] T. Kodama, S. Komarneni, J. Mater. Chem. 9 (1999) 2475-2480.

[10] M. Park, D. H. Lee, C. L. Choi, W. T. Lim, S. K. Lee, N. H. Heo, S. Komarneni, J. Choi, J. Porous Mater. 9 (2002) 291-298.

[11] M. Park, D. H. Lee, C. L. Choi, S. S. Kim, K. S. Kim, J. Chem. Mater. 14 (2002) 2582-2589.

[12] M. Naranjo, M. A. Castro, A. Cota, E. Pavón, M. C. Pazos, M. D. Alba, Micro. Mes. Mater. 186 (2014) 176-180.

[13] M. D. Alba, A. I. Becerro, M. A. Castro, A. C. Perdigón, Am. Miner. 86 (2001) 115-123.

[14] A. Moronta, Inter. Sci. Tech. 1 (2004) 321-344.

[15] G. Engelhardt, D. Michel, High-Resolution Solid-State NMR of Silicates and Zeolites, John Wiley & Sons, New York, 1987.

[16] J. T. Kloprogge, M. Hammond, L. Hickey, R. L. Frost, J. Mater. Sci. Lett. 21 (2002) 931-933.

[17] A. Decarreau, O. Grauby, S. Petit, Appl. Clay Sci. 7 (1992) 147-167.

[18] F. Muller, G. Besson, A. Manceau, V. A. Drits, Phys. Chem. Miner. 24 (1997) 159-166.

[19] M. Jaber, J. Miehé-Brendlé, Micr., Mes. Mater. 107 (2008) 121-127.

[20] J. T. Kloprogge, L. Hickey, R. L. Frost, J. Mater. Sci. Lett. 18 (1999) 1401-1403.

[21] D. Zhang, C. H. Zhou, C. X. Lin, D. S. Tong, W. H. Yu, Appl. Clay Sci. 50 (2010) 1-11.

[22] M. D. Alba, M. A. Castro, M. Naranjo, M. M. Orta, E. Pavón, M. C. Pazos, J. Phys. Chem. C 115 (2011) 20084-20090.

[23] J. T. Kloprogge, J. Breukelaar, J. B. H. Jansen, J. W. Geus, Clays Clay Miner. 41 (1993) 103-110.

[24] E. J. Palin, M. T. Dove, A. Hernandez-Laguna, C. I. Sainz-Diaz, Amer.Miner. 89 (2004) 164-175.

[25] V. McGahay, M. Tomozawa, J. Non-Crys. Sol. 109 (1989) 27-34.

[26] H. Kalo, M. W. Möller, M. Ziadeh, D. Dolejš, J. Breu, Appl. Clay. Sci. 48 (2010) 39-45.

[27] D. Massiot, F. Fayon, M. Capron, I. King, S. LeCalvé, B. Alonso, J.O. Duran, B. Bujoli, Z. Gan, G. Hoatson, Magn. Reson. Chem. 40 (2002) 70-76.

[28] G. W. Brindley, G. Brown, Crystal structures of Clay Minerals and their X-ray identification, Mineralogical Society, London, 1980, 495 pp.

[29] B.E. Warren, Phys. Rev. 59 (1941) 693-698.

[30] G. Engelhardt, D. Michel, High-Resolution Solid-State NMR of Silicates and Zeolites, John Wiley & Sons, New York, 1987.

[31] J.G. Thompson, R.L. Withers, A.K. Whittaker, R. M. Trail, J. D. Fitz Gerald, J. Solid Stat. Chem. 104 (1993) 59-73.

[32] M. D. Alba, A. I. Becerro, M. A. Castro, A. C. Perdigón, Am. Miner. 86 (2001) 124-131.

[33] E. Lippmaa, A. Samoson, M. Mägi, J. Am. Chem. Soc. 108 (1986) 1730-1735.

[34] A. Kutoglu, Z. Kristallogr. 199 (1992) 197-201.

[35] G.M. Johnson, P. J. Mead, S. E. Dann, M. T. Weller, J. Phys. Chem. B 104 (2000) 1454-1463.

[36] H. Hill, H. Eckert, V.I. Srdanov, J. Phys. Chem. B 107 (2003) 8779-8788.

[37] R. J. M. J. Vogels, J. T. Kloprogge, J. W. Geus, Am. Miner. 90 (2005) 931-944.

[38] R. E. Grim, Clay Mineralogy, McGraw-Hill Book Company, New York, 1968.

[39] R. C. Mackenzie, Nature 181 (1958) 334-334.

[40] Z. Zeng, D. Matuschek, A. Studer, C. Schwicker, R Pöttgen, H Eckert, Dalton Trans. 42 (2013) 8585-8596.

[41] B. Casal, P. Aranda, J. Sanz, E. Ruiz-Hitzky, Clay Miner. 29 (1994) 191-203.

1

Table 1.

Crystalline phases evolution.

T (ºC)	S	DM	HM	F	N	s	A	n
600								
650								
700								
750								
775								
800								
850								
900								

S=Saponite; DM=Dehydrated Na-Mica; HM=Hydrated Na-Mica; F=Forsterite; N=Norbergitte; s=sodalite; A=Aluminum oxide fluoride; n=Neighborite

2:1 phyllosilicate (Q^3)
Nesosilicates (Q^0)
Tectosilicates (Q^4)
fluorides

Table 2.

^{29}Si chemical shifts (δ), line widths (fwhh), quantifications (%) and assignation of signals obtained by fitting ^{29}Si MAS NMR spectra of the products.

T (ºC)	δ (ppm)	fwhh (Hz)	%	assignation
600	-61.1	92.2	5.5	Q^0
	-89.0	195.5	0.4	Saponite, Q^3(1Al)
	-95.3	234.5	40.8	Saponite, Q^3(0Al)
	-105.8	1473.3	41.3	Q^4(1Al)
	-112.0	649.8	12.1	Q^4(0Al)
650	-60.8	314.8	3.9	Q^0
	-82.2	847.4	6.3	Q^3(3Al)
	-84.6	161.0	0.9	Q^3(2Al) + sodalite
	-89.6	282.0	18.5	Q^3(1Al)
	-95.1	247.9	66.0	Q^3(0Al)
	-108.1	742.3	4.4	Q^4(1Al)
700	-79.2	147.2	0.5	Q^3(3Al)
	-84.6	409.4	11.9	Q^3(2Al) + sodalite
	-89.6	244.2	30.8	Q^3(1Al)
	-94.8	229.3	56.9	Q^3(0Al)
750	-61.8	342.3	2.4	Q^0
	-77.7	197.9	3.2	Q^3(3Al)
	-84.6	484.1	13.1	Q^3(2Al) + sodalite
	-89.6	246.5	35.2	Q^3(1Al)
	-94.4	214.9	46.1	Q^3(0Al)
775	-61.2	103.4	4.2	Q^0
	-75.1	394.1	1.4	Q^3(3Al)[a]/Q^2
	-78.0	131.7	7.6	Q^3(3Al)
	-82.4	265.8	29.0	Q^3(2Al)
	-88.6	286.1	36.1	Q^3(1Al)
	-93.5	185.2	21.7	Q^3(0Al)
800	-60.3	654.9	2.9	Q^0
	-71.5	362.3	0.4	Q^3(3Al)[a]/Q^2
	-77.9	166.1	28.1	Q^3(3Al)
	-82.1	235.7	29.6	Q^3(2Al)
	-86.0	348.5	20.6	Q^3(1Al) + sodalite
	-89.1	254.6	13.1	Q^3(0Al)
	-93.5	192.2	5.3	Q^3(0Al)
850	-61.4	204.8	0.5	Q^0
	-74.8	128.4	5.2	Q^3(3Al)[a]Q^2
	-77.6	178.1	36.8	Q^3(3Al)
	-81.7	225.5	26.3	Q^3(2Al)
	-85.8	535.7	31.2	Q^3(1Al)
900	-62.1	167.5	1.8	Q^0
	-75.0	125.6	4.7	Q^3(3Al)[a]/Q^2
	-77.5	120.6	49.1	Q^3(3Al)
	-81.5	206.0	37.0	Q^3(2Al)
	-85.8	186.1	4.9	Q^3(1Al)
	-89.6	318.6	2.5	Q^3(0Al)

[a] Q^3(3Al) with Al-O-Al bonding, Lowenstein´s rule violation.

1

1

Table 3.

Temperature and weight loss of the dehydration reaction

T (ºC)	T^{DTA} (ºC)	Weight $loss^{TG}$ (%)
600	32.6 61.9	2.7
650	69.4	3.0
700	69.1	3.4
750	65.3	4.1
775	70.4	4.0
800	80.1	5.9
850	81.7	5.9
900	75.3	6.9

1

Table 4.

^{23}Na chemical shifts (δ), line widths (fwhh), quantifications (%) and assignation of signals obtained by fitting ^{23}Na MAS NMR spectra of the products.

T (ºC)	δ (ppm)	fwhh (Hz)	% total	% mica Na	assignation
600	37.2	722.6	6.2	6.4	non exchangeable
	3.7	1021.85	3.6		sodalite
	-10.1	1409.84	32.8		Fully hydrated exchangeable
	-21.1	1777.11	35.2	93.6	Poorly hydrated exchangeable
	-33.2	3267.87	22.2		Dehydrated exchangeable
650	36.5	844.6	7.6	4.2	non exchangeable
	5.1	469.4	3.9		sodalite
	-10.7	1359.4	48.5		Fully hydrated exchangeable
	-22.0	1628.5	20.1	95.8	Poorly hydrated exchangeable
	-33.0	2800.5	20.0		Dehydrated exchangeable
700	34.7	940.5	6.3	6.7	non exchangeable
	4.9	419.0	5.9		sodalite
	-10.9	1214.5	53.1	93.3	Fully hydrated exchangeable
	-19.0	3739.4	34.7		Poorly hydrated exchangeable
750	34.5	962.7	7.3	8.1	non exchangeable
	5.0	429.6	11.2		sodalite
	-9.8	1157.4	80.9	91.9	Fully hydrated exchangeable
	-29.7	1419.7	1.5		Dehydrated exchangeable
775	34.9	799.0	7.7	8.5	non exchangeable
	5.7	313.9	9.0		sodalite
	-9.0	839.6	63.0	91.5	Fully hydrated exchangeable
	-22.9	3576.4	20.3		Poorly hydrated exchangeable
800	32.9	1528.4	3.8	3.8	non exchangeable
	5.4	307.4	1.2		sodalite
	-8.1	606.4	72.8	96.2	Fully hydrated exchangeable
	-11.0	1217.9	22.2		
850	28.5	1154.4	1.2	1.2	non exchangeable
	5.9	271.6	0.1		sodalite
	-8.0	685.7	75.9	98.8	Fully hydrated exchangeable
	-18.3	1477.7	22.8		Poorly hydrated exchangeable
900	30.6	1217.0	0.5	0.5	non exchangeable
	5.7	475.4	0.1		sodalite
	-7.9	741.8	82.9		Fully hydrated exchangeable
	-14.3	1865.2	16.5	99.5	Poorly hydrated exchangeable

FIGURE CAPTION

Fig. 1. (a) Total weight loss after calcination and (b) net weight change after washing process, as a function of the calcination temperature. Dash line=theoretical weight loss due to calcination (eq. I), dotted line=theoretical net weight change due to the NaCl excess (eq. II), and, solid line= theoretical net weight change due to the NaCl removal and hydration (eq. III).

Fig. 2. XRD patterns of the samples as a function of calcination temperature (top) and reflections of the reference patterns (bottom). The lines on the top figure indicate the characteristic reflections of trioctahedral smectites (dot line) and the fluoromica Na-Mica-4 (dash and dash-and-dot lines).

Fig. 3. ^{29}Si and ^{27}Al MAS NMR spectra of the samples as a function of the calcination temperature.

Fig. 4. ^{23}Na MAS NMR spectra of the samples as a function of the calcination temperature.

1 *Figure 1*

2

3

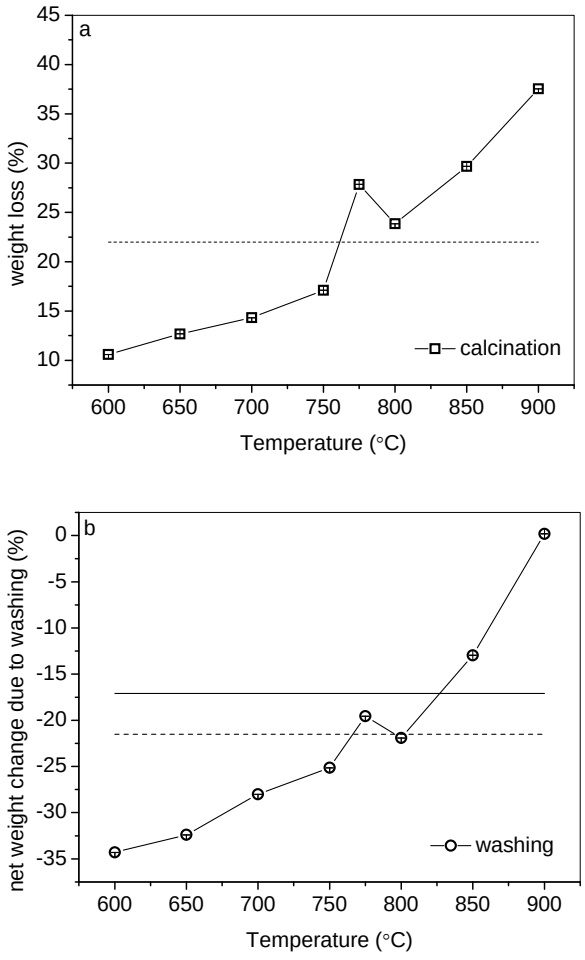
a
weight loss (%)
Temperature (°C)
calcination
b
net weight change due to washing (%)
Temperature (°C)
washing

Figure 2

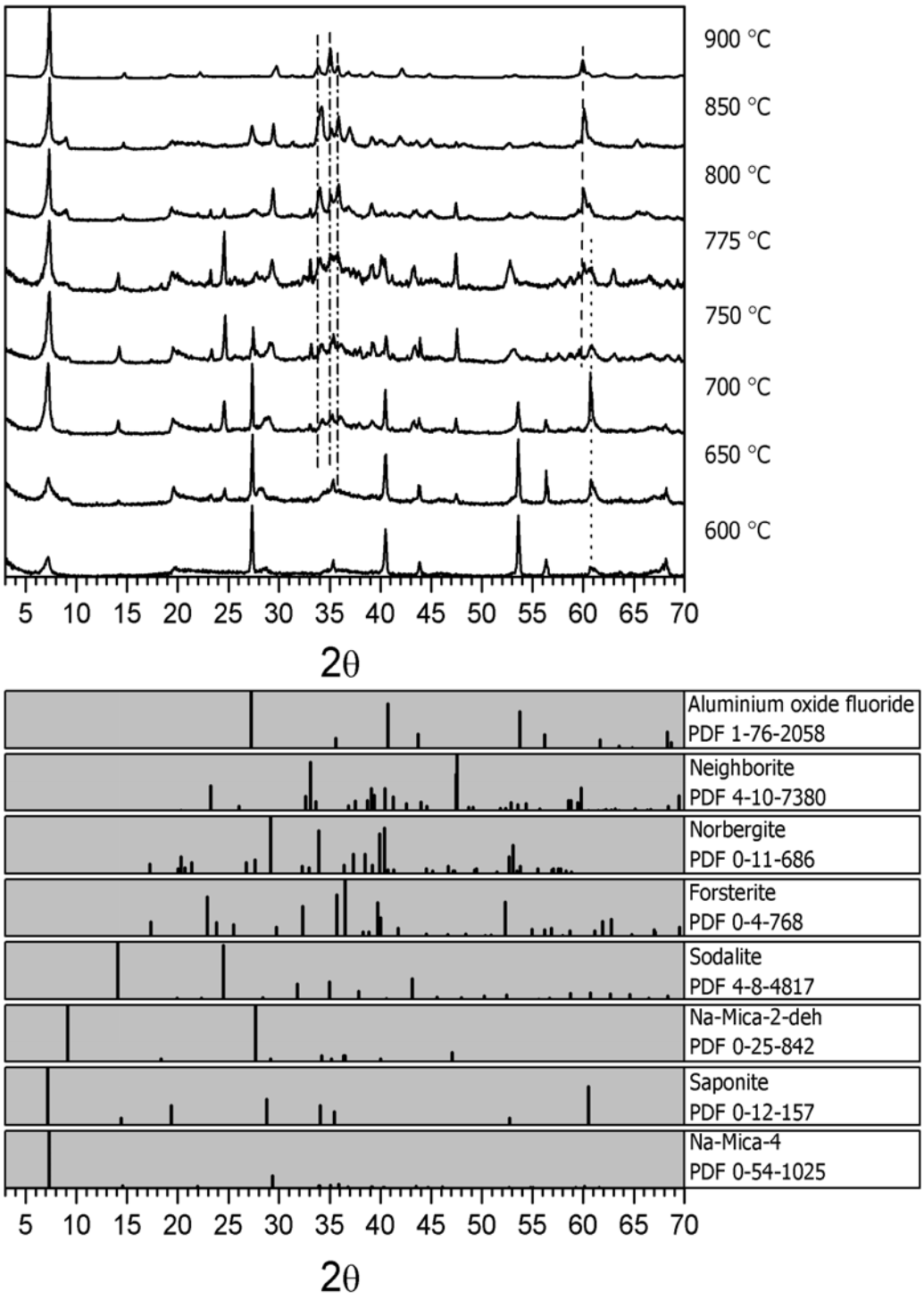
900 °C
850 °C
800 °C
775 °C
750 °C
700 °C
650 °C
600 °C
5 10 15 20 25 30 35 40 45 50 55 60 65 70
2θ
Aluminium oxide fluoride
PDF 1-76-2058
Neighborite
PDF 4-10-7380
Norbergite
PDF 0-11-686
Forsterite
PDF 0-4-768
Sodalite
PDF 4-8-4817
Na-Mica-2-deh
PDF 0-25-842
Saponite
PDF 0-12-157
Na-Mica-4
PDF 0-54-1025
5 10 15 20 25 30 35 40 45 50 55 60 65 70
2θ

Figure 3

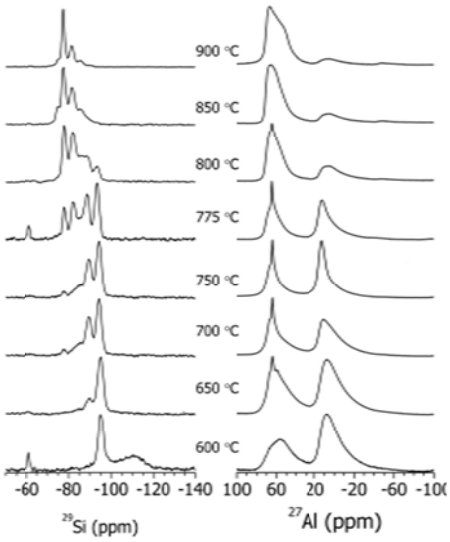
900 °C
850 °C
800 °C
775 °C
750 °C
700 °C
650 °C
600 °C
-60 -80 -100 -120 -140
29Si (ppm)
100 60 20 -20 -60 -10
27Al (ppm)

Figure 4

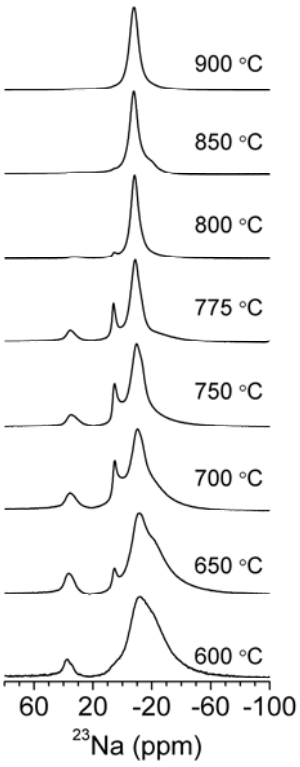
900 °C
850 °C
800 °C
775 °C
750 °C
700 °C
650 °C
600 °C
60 20 -20 -60 -100
^{23}Na (ppm)

Suppl. 1. Evolution of ^{29}Si MAS NMR signal as a function of the synthesis temperature. *= Q^3(3Al) signal overlaps with sodalite signal